Alkyl side chain impact on the charge transport and photovoltaic properties of benzodithiophene and diketopyrrolopyrrole-based copolymers

Li, Zhao; Zhang, Yanguang; Tsang, Sai-Wing; Du, Xiaomei; Zhou, Jiayun; Tao, Ye; Ding, Jianfu

Publisher's version / Version de l'éditeur:
https://doi.org/10.1021/jp202996p
The journal of physical chemistry. C, 115, 36, pp. 18002-18009, 2011-08-08

THE JOURNAL OF PHYSICAL CHEMISTRY C

ARTICLE

pubs.acs.org/JPCC

Alkyl Side Chain Impact on the Charge Transport and Photovoltaic Properties of Benzodithiophene and Diketopyrrolopyrrole-Based Copolymers§

Zhao Li,*,† Yanguang Zhang,‡ Sai-Wing Tsang,‡ Xiaomei Du,† Jiayun Zhou,‡ Ye Tao,‡ and Jianfu Ding*,†

†Institute for Chemical Process and Environmental Technology (ICPET) and ‡Institute for Microstructural Sciences (IMS), National Research Council of Canada (NRC), 1200 Montreal Road, Ottawa, ON, Canada, K1A 0R6

ABSTRACT: To investigate the side chain effect on the photovoltaic performance of conjugated copolymers with alternating electron push−pull structures, three alternating copolymers (O−HD, BO−BO, and PU−O) of benzodithiophene and dithienyldiketopyrrolopyrrole were designed and synthesized. They were nomenclated based on the side chains on the benzodithiophene (BDT) and the diketopyrrolopyrrole (DPP) units, which are octyl (O) and 2-hexyldecyl (HD); 3-butyloctyl (BO), and 2-butyloctyl (BO): and 3-pentylundecyl (PU) and octyl (O) groups, respectively. The total C number of the side chains in each repeat unit was kept at 48 to control the dilute effect. The solubility, optical, and electrochemical properties, and crystalline structure of the polymers were depended on the combination of these linear or branched alkyl chains. Thin film transistor (TFT) characterization showed that PU−O had the best hole mobility up to 1.6×10^{-3} cm^2V^{-1} s^{-1}. The best photovoltaic performance was observed from O−HD with power conversion efficiency (PCE) up to 4.1%. However, it only showed a modest hole mobility of 3.8×10^{-4} cm^2V^{-1} s^{-1}, about 4-fold lower than PU−O. This dramatically different performance of these polymers for TFT and photovoltaic devices was explained by the interaction at the interface of the polymer electron donor and the PCBM acceptor domains.

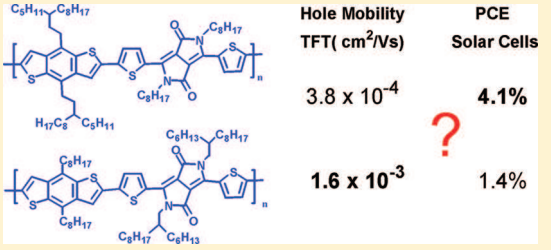

INTRODUCTION

Compared with inorganic materials, the most promising advantage of conjugated polymers for electronics is their solution processability, which makes them compatible with existing large scale and low cost fabrication techniques, such as roll-to-roll and ink jet printing.[1] To make these conjugated polymers soluble in organic solvents, alkyl side chains are usually introduced onto their main chains. However, these nonconjugated groups will dilute the functional main chain in the organic semiconductors. Moreover, the position, length, and bulkiness of these alkyl chains will dramatically influence the aggregation behavior of these materials in solid state, thus impact their optical and electronic properties.[1]

One of the most extensively studied conjugated polymers is poly(3-alkylthiophene)s (P3AT).[2] The successful synthesis of regioregular poly(3-hexylthiophene) (rr-P3HT) represents a landmark for the development and application of P3AT.[3] The high regioregular chain conformation of rr-P3HT renders this polymer a high degree of intermolecular ordering in solid state and thus offers the material a lower band gap and enhanced charge carrier mobility as compared with random P3HT.[3] The side chain effect has also been extensively studied for P3AT. Gadisa et al. studied the effect of alkyl side chain length on the photovoltaic properties of P3AT/PCBM-based bulk heterojunctions.[4] Jenekhe et al. found that the multiple side chains in P3AT can fine-tune its optoelectronic properties.[5] Hou and Yang et al. reported that the molecular energy levels of P3AT can be effectively modulated by adjusting the side chain architecture.[6]

To further lower the band gap and improve the absorption of conjugated polymers, copolymers containing alternating electron-rich and electron-deficient units are developed to form electron push−pull structures.[1] Because of delocalized π-electrons and formation of quinoidal structures, these copolymers usually exhibit a narrower band gap in addition to deeper LUMO and HOMO energy levels. For photovoltaic applications, a narrow band gap means a broader light absorption and subsequently an improved short-circuit current density (J_{sc}). A deeper HOMO of polymer means a larger offset from LUMO of fullerene derivatives and will result in a higher open circuit voltage (V_{oc}). Indeed, high-performance polymer solar cells with power conversion efficiency (PCE) over 6% have been fabricated based on these materials.[7] This kind of push−pull structure can also enhance the interaction between polymer chains and results in materials with high charge carrier mobility for field effect transistor (FET) applications.[8] Similar to the case of P3AT, the choice of alkyl side chains on these copolymers will also influence their solubility, $\pi-\pi$ stacking, and other optical and electronic properties. However, because of the existence of a wide range of electron-rich and electron-deficient building blocks, and a large number of side chains to attach at different positions of these building blocks, the impact of the side chain is more complicated. Detailed study and comparison of the effect of different alkyl

Received: March 31, 2011
Revised: July 4, 2011
Published: August 08, 2011

chains on the properties of these copolymers are limited.[9] Herein, we chose two commonly utilized building units, benzodithiophene (BDT) and diketopyrrolopyrrole (DPP). We introduced different linear or branched alkyl chains on BDT or DPP units to obtain three copolymers, and compared their solubility, optical, electrochemical properties, and crystalline structures. We correlated their different FET and photovoltaic behavior with their side chain structure and hope our work can shed light on the design of new organic electronic materials with optimized side chain architecture.

RESULTS AND DISCUSSION

Polymer Synthesis and Characterization. As shown in Scheme 1, the polymers were synthesized by Stille coupling reaction. Both electron-rich BDT and electron-deficient DPP units have been utilized to prepare high-performance organic electronic materials.[7a,e,f,8a,8d,10] The bis(trimethyltin) compounds of BDT and dibromides of dithienyl DPP were synthesized as reported.[11] The polymers were nomenclated according to the substituted groups on BDT and DPP units as illustrated in Scheme 1. Although the size and shape of the alkyl side chains on BDT and DPP units varied in the three polymers, they all contain a sum of 48 carbon atoms in the alkyl side chains to eliminate complications from dilution of conjugated moiety.[9] Gel permeation chromatography (GPC) analysis reveals that all three polymers have high molecular weight with number average molecular weight (M_n) over 25 kDa and polydispersity index (PDI) around 2.0 after a careful purification of solvent extraction. The thermal transition and stability of the polymers were investigated with differential scanning calorimetry (DSC) and thermal gravimetric analysis (TGA). DSC analysis did not reveal any glass transition and melting process with the temperature up to 350 °C. Combining with the XRD study shown later, this result indicates that the polymers are highly crystalline and the melting points are higher than 350 °C. TGA curves show that a degradation temperature with 2% weight loss are ~390 °C. The characterization data are summarized in Table 1.

Scheme 1. Synthesis of the Conjugated Polymers

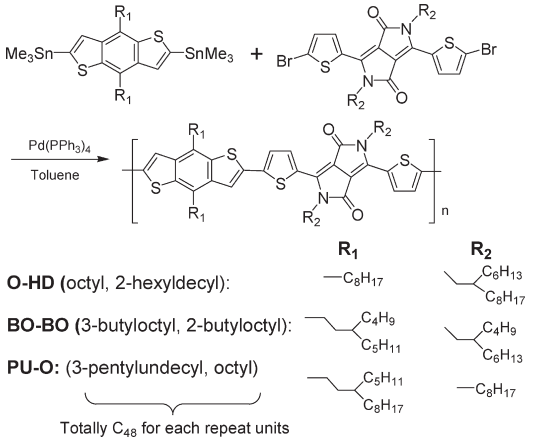

Optical Properties and Solubility. The photophysical properties of the polymers are investigated by UV−vis spectra of dilute chlorobenzene solutions and thin films as shown in Figure 1. All of the polymers show three absorption bands with the maxima near 400, 690, and 760 nm. It is interesting that in the dilute solution, polymer O−HD shows highest molar absorption coefficient of 1.15×10^{-5} $M^{-1}cm^{-1}$, compared with 1.01×10^{-5} $M^{-1}cm^{-1}$ and 0.78×10^{-5} $M^{-1}cm^{-1}$ for BO−BO and PU−O respectively, although these polymers share the same backbone and the same side chain carbon numbers for each repeat unit. Comparatively, the thin films show broader absorption curve because of stronger interchain interaction in the solid state.

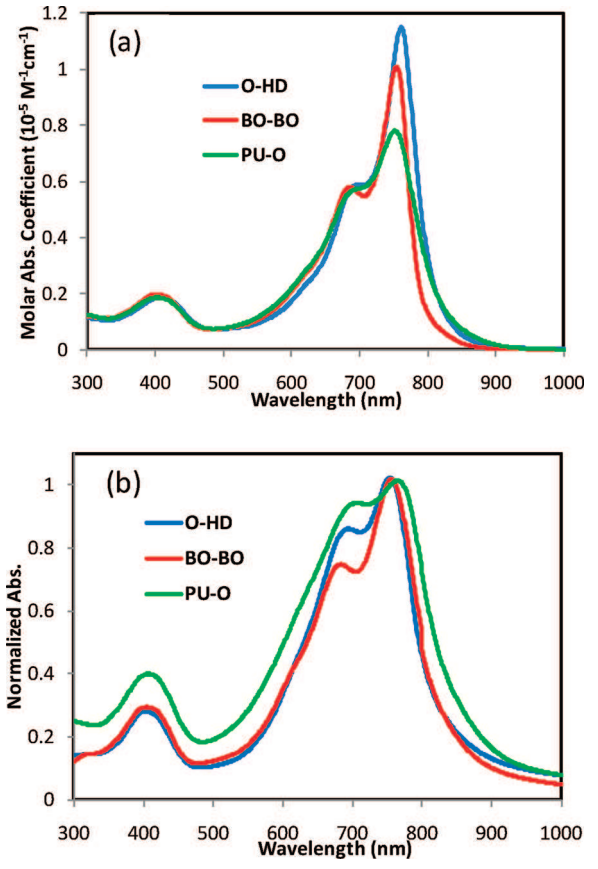

Figure 1. UV absorption spectra of the (a) dilute chlorobenzene solution and (b) thin film of the polymers.

Table 1. Polymer Characterization

polymer	M_n [kDa][a]	PDI[a]	T_d [°C][b]	soln λ_{max} [nm][c]	film λ_{max} [nm]	E_g^{opt} [eV][d]	E_{os}^{red} [V][e]	E_{os}^{ox} [V][e]	LUMO [eV][f]	HOMO [eV][f]
O−HD	42.8	2.14	390	762	754	1.45	−1.10	0.77	−3.28	−5.15
BO−BO	33.2	2.48	382	754	756	1.51	−1.04	0.76	−3.34	−5.14
PU−O	27.8	1.97	395	753	766	1.36	−1.07	0.72	−3.31	−5.10

[a] Number average molecular weight and polydispersity index (GPC vs polystyrene standards in chlorobenzene). [b] Temperature for 2% weight loss from TGA curve. [c] Solution absorption in chlorobenzene. [d] Optical energy gap estimated from the onset of UV curve measured in thin film. [e] Onset potentials from CV measurements of thin films in 0.1 M Bu_4NPF_6/CH_3CN solution vs Ag. [f] Estimated from $E_{LUMO} = -(E_{os}^{red} + 4.38)$ eV and $E_{HOMO} = -(E_{os}^{ox} + 4.38)$ eV.

dx.doi.org/10.1021/jp202996p | J. Phys. Chem. C 2011, 115, 18002–18009

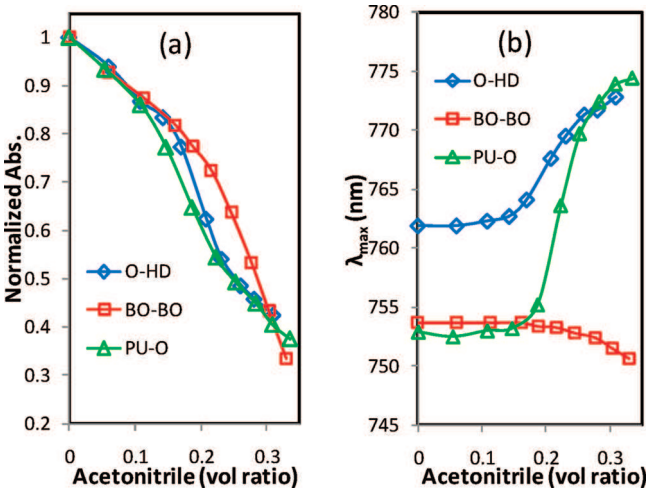

Figure 2. Shift of (a) normalized absorption and (b) the λ_{max} of the UV−vis spectra of polymer chlorobenzene solutions (1×10^{-5} M) with the addition of acetonitrile.

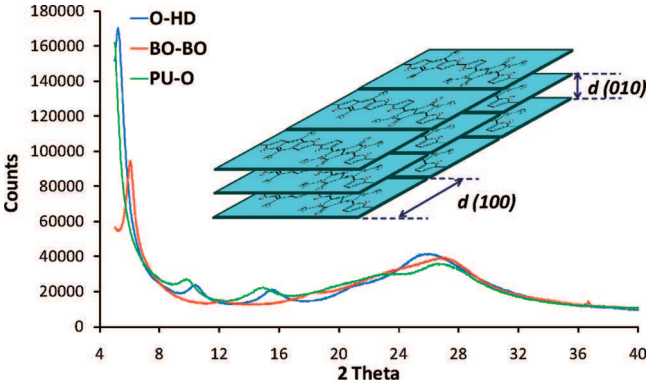

Figure 3. XRD spectra of polymer films (insert, schematic lamellar structure).

As expected, polymer BO−BO, containing only branched side chains, shows the best solubility in the three polymers. It is soluble in THF, chloroform, toluene, and chlorobenzene at 21 °C, whereas O−HD and PU−O are only slightly soluble in these solvents at 21 °C but can dissolve in chloroform, toluene, and chlorobenzene at higher temperatures. This solubility difference was also confirmed by a UV test in a mixture solvent. Therefore, a nonsolvent, acetonitrile was slowly added into the dilute chlorobenzene solutions (1×10^{-5} M) of these polymers, and their UV−vis spectra were monitored. As shown in Figure 2, as the volume ratio of acetonitrile increased, the absorption intensity of BO−BO solution decreased due to the dilution of the solution and the maximum absorption peak (λ_{max}) slightly decreased from 754 to 750 nm due to change of solvent polarity. However, during the addition of acetonitrile, the other two polymers showed a different behavior. The absorption intensity and λ_{max} both showed S-shaped curve with the addition of acetonitrile. At 15 vol % of acetonitrile, O−HD and PU−O showed an abrupt drop in absorption with the maximum dramatically shifted to longer wavelength, indicating the occurrence of chain aggregation. It should be noted that although the chain aggregation in this mixture solvent shifted λ_{max} of O−HD from 762 nm and PU−O from 753 to 774 nm, the aggregation in film did not create any apparent λ_{max} shift. The reason of this phenomenon is still under investigation.

Table 2. Diffraction Angles and *d*-Spacing Calculated form XRD Spectra

	2θ (degree)/*d*-spacing (Å)			
polymers	(100)	(200)	(300)	(010)
O−HD	5.23/19.6	10.41/19.7	15.55/19.8	25.22/4.09
BO−BO	6.04/16.9	12.08/17.0		26.35/3.92
PU−O		9.8/20.9	14.82/20.8	26.02/3.97

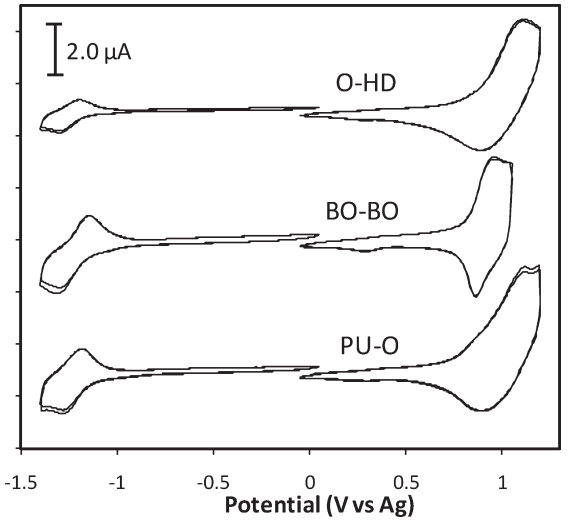

Figure 4. Cyclic voltammogram of polymer films coated on a platinum electrode in Bu_4NPF_6/CH_3CN solution.

X-ray Diffraction (XRD) and Electrochemical Properties. It is well-known that solid state packing will dramatically influence the electronic properties of conjugated polymers.[12] XRD are employed to investigate the crystalline structure of the polymer films, the curves are shown in Figure 3 and data are summarized in Table 2. Distinct primary diffraction features are observed at 2θ of 5.23°, and 6.04°, corresponding to *d*(100) spacings of 19.6 and 16.9 Å for polymers O−HD and BO−BO, respectively. The *d*(100) spacing of polymer PU−O can be calculated from the second and third-order peaks of its XRD curve to be 20.9 Å. The *d*(100) spacing increases from 16.9, 19.6, to 20.9 Å as the longest side chains increased from C8, C10 to C11 for polymer BO−BO, O−HD, and PU−O (Figure 3). Polymers O−HD and PU−O exhibit crystalline patterns with diffraction peaks up to third-order, whereas BO−BO only reveals a vague second-order peak, indicating a higher degree of solid state ordering of O−HD and PU−O. However, all three polymers show similar π−π stacking peak with distance of ~4 Å between stacked aromatic backbones.

The electrochemical properties of these polymers are investigated with cyclic voltammetry (CV) and the curves are shown in Figure 4 with the data summarized in Table 1. All polymers undergo reversible reductive *n*-doping/dedoping and reversible oxidative *p*-doping/dedoping processes. They have similar onset potentials for reductive and oxidative peaks at −1.07 and 0.75 V, corresponding to LUMO and HOMO energy levels at −3.31 eV and −5.13 eV, respectively showing that the different alkyl

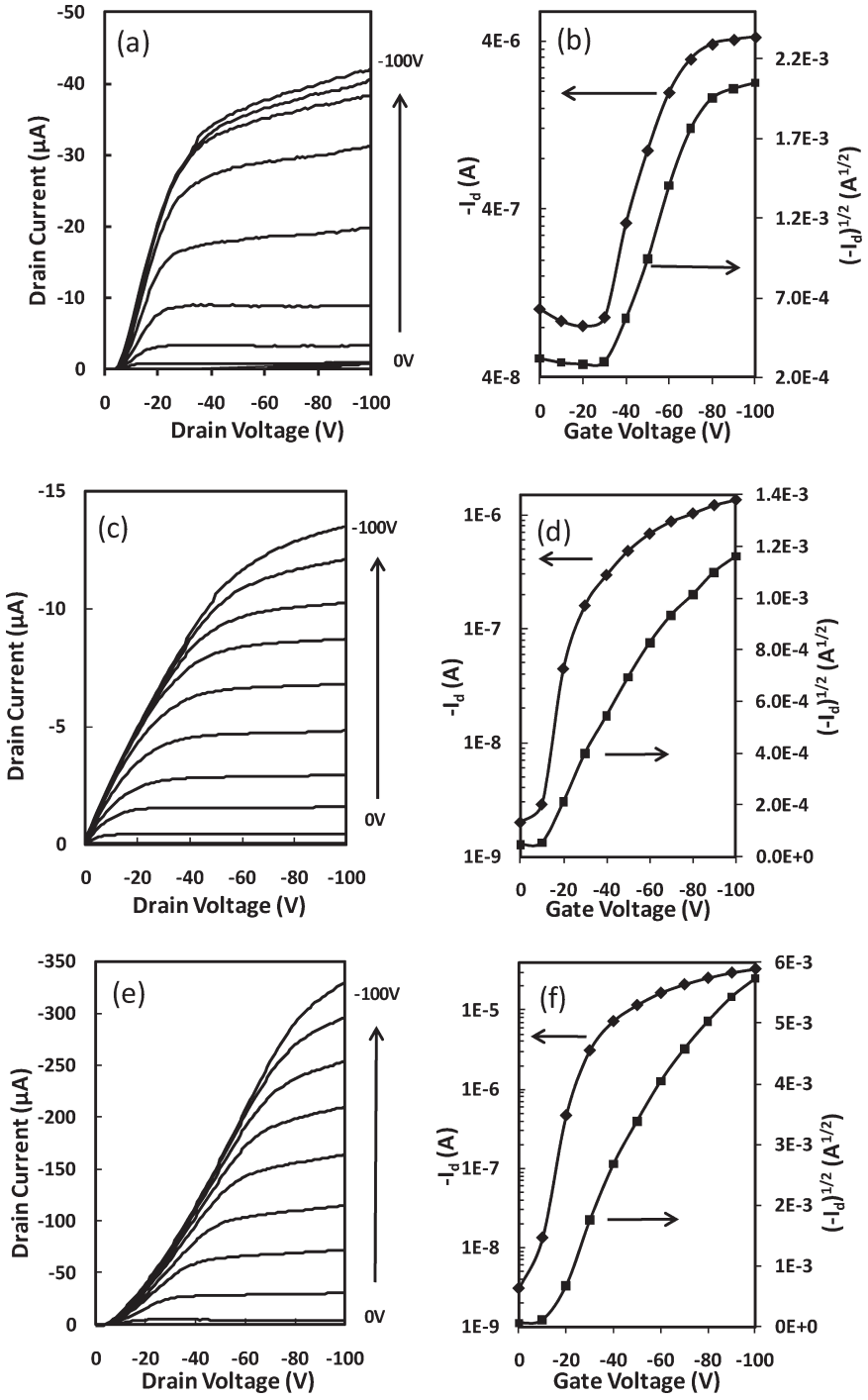

Figure 5. Representative I−V curves and output characteristics of *p*-type OFET devices of O-HD (a, b), BO-BO (c, d), and PU-O (e, f) tested in a glovebox.

chains have minor effect on their electrochemical properties. Comparatively, the area of oxidative *p*-doping/dedoping peak is substantially larger than the reductive *n*-doping/dedoping peak indicating stronger electron donating capacity than that of electron accepting. The half wave current of the reductive peak for polymer O−HD is about 1.3 μA, compared with 2.6 and 2.3 μA for polymer BO−BO and PU−O. The electron deficient part in an alternating copolymer usually determines its electron accepting capability. The bulkier branched alkyl chain on the electron deficient DPP unit in polymer O−HD may create a larger resistance for the DPP units to accepting electrons in the reductive process leading to a reduced half wave current.

Field Effect Transistor (FET) Characterization. The field effect mobility of these polymers was investigated using bottom-contact organic FET. As shown in Figure 5, all of the transistors exhibited typical *p*-type behavior and distinct field effects were observed from the output characteristics. The hole mobilities without intensive optimization are estimated to be 3.8×10^{-4}, 5.9×10^{-5}, and 1.6×10^{-3} $cm^2/(V\ s)$ for O−HD, BO−BO, and PU−O, respectively. The FET characterization data were

summarized in Table 3. Polymers O−HD and PU−O show higher mobility. This agrees well with the crystallinity results obtained from UV and XRD measurements, as they show stronger tendency to aggregate in poor solvents and more distinct diffraction patterns in the solid film. Polymer PU−O yielded devices with a hole mobility of 1.6×10^{-3} $cm^2/(V\,s)$, a factor of 4−5 higher than that of O−HD indicating DPP units can create stronger interchain interaction than BDT units.[13]

Photovoltaic Performance and Atomic Force Microscopy (AFM). Polymer solar cells were fabricated from these polymers and (6, 6)-phenyl-C_{71} or C_{61}-butyl acid methyl ester (PCBM) with a general device structure of ITO/PEDOT:PSS/polymer:PCBM/LiF/Al. Different processing conditions, such as choice of solvents, spin coating temperature and using of additives, were tested to optimize the device performance. Typical current density−voltage ($J-V$) curves are shown in Figure 6 and the device performance data with the fabrication conditions are listed in Table 4. Briefly, the device fabricated from the blend of O-HD and $PC_{71}BM$ in dichlorobenzene containing 2.5% diiodooctane at 70 °C gives the best photovoltaic performance with a V_{oc} of 0.71 V, a J_{sc} of 9.4 mA/cm^2, and a fill factor (FF) of 61%; the PCE thus reached 4.1%, which is slightly higher than the data from the polymer with the same main chain structure, with alkoxy instead of alkyl side chains attached to the BDT unit,[11d] where the more flexible alkoxy group offer the polymer a higher solubility so that smaller side group can be used to obtain a similar solubility.[11d] Under the same fabrication condition, devices from polymer BO−BO and PU−O only give PCE of 0.93% and 1.4%, respectively.

The external quantum efficiency (EQE) and the total absorption (1-reflectance) of devices from O−HD at different wavelength are shown in Figure 7. The absorption from these blends covers a wide range from 300 to 850 nm, and device D3 from blends of O−HD with $PC_{71}BM$ shows higher EQE and stronger absorption between 400 and 800 nm, due to the enhanced absorption from the contribution of $PC_{71}BM$. The integrated J_{sc} is close to that from the $J-V$ curve, demonstrating the spectral mismatch is small.

Tapping mode AFM was utilized to observe the surface morphological structure of the active layer and the phase images are shown in Figure 8. The film on device D3 shows uniform and distinct phase separated structure. The bright grains with size around 20 nm can be assigned to O−HD, which forms channels in the fullerene matrix. This interpenetrated network structure is highly desirable for the active layer of photovoltaic devices and can explain the superior performance of D3. The active layer from D5 and D6 shows obscure and large domains with less clear phase separated structure corresponding to modest FF and PCE of these two devices.

Interaction within and between Electron Donor and Electron Acceptor. The poor photovoltaic performance of BO−BO can be explained by its low hole mobility and slightly poor crystalline structure formed during the spin coating process. However, polymer PU−O has the best charge carrier mobility

Table 3. OFET Characterization of the Polymers in N_2

polymer	μ, $cm^2/(V\,s)$	$I_{on/off}$	V_{th}, V
O−HD	3.8×10^{-4}	4.1×10^{1}	−23.4
BO−BO	5.9×10^{-5}	6.7×10^{2}	−4.8
PU−O	1.6×10^{-3}	1.1×10^{4}	−8.1

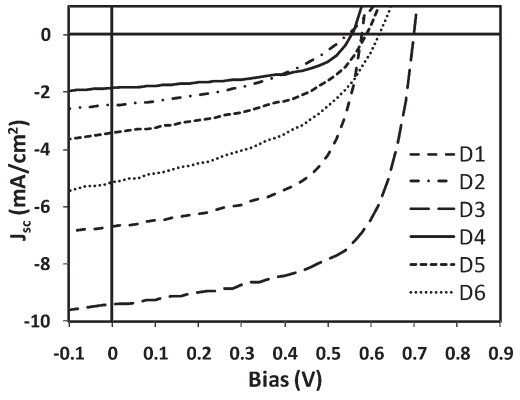

Figure 6. $J-V$ curve of polymer/PCBM (weight ratio 1:2) bulk heterojunction solar cells under illumination of AM 1.5G, 100 mW cm^{-2}, Table 4 for device fabrication conditions.

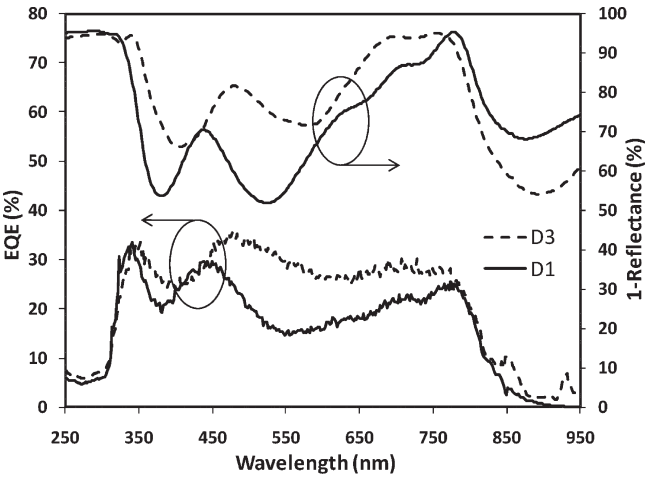

Figure 7. EQE spectra and 1-reflectance spectra of devices **D1** and **D3**.

Table 4. Summary of Device Fabrication and Photovoltaic Performance

devices	polymer/PCBM[a]	DIO[b] (%)	temp[c] (°C)	J_{sc}[d] (mA/cm^2)	V_{oc} (V)	FF (%)	PCE[d] (%)
D1	O−HD/$PC_{61}BM$	0	21	6.7 (6.1)	0.59	57	2.3 (2.1)
D2	O−HD/$PC_{71}BM$	0	70	2.5	0.55	42	0.57
D3	O−HD/$PC_{71}BM$	2.5	70	9.4 (8.8)	0.71	61	4.1 (3.9)
D4	BO−BO/$PC_{61}BM$	0	21	1.9	0.55	57	0.58
D5	BO−BO/$PC_{71}BM$	2.5	70	3.4	0.59	46	0.93
D6	PU−O/$PC_{71}BM$	2.5	70	5.2	0.62	43	1.4

[a] Polymer/PCBM weight ratio is 1:2. [b] Volume ratio of 1,8-diiodooctane to dichlorobenzene. [c] Device fabrication temperature. [d] EQE calculated data are shown in bracket.

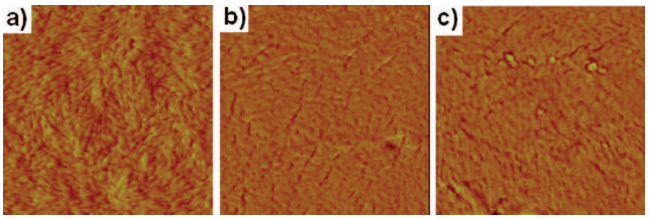

Figure 8. AFM phase images of active layer on devices (a) D3, (b) D5, and (c) D6. The size of images is 1 × 1 μm^2.

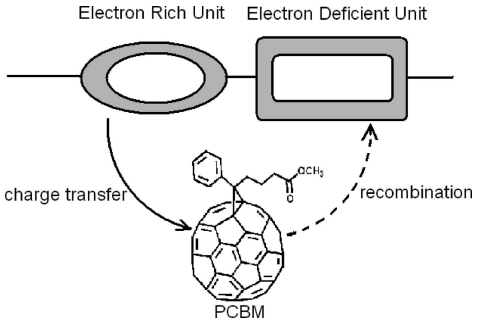

Figure 9. Possible interaction between polymer and PCBM, charge transfer, and recombination pathway are shown by arrows. Gray region represents alkyl side chains.

among three polymers and similar chain packing behavior as O−HD. It is surprising that this polymer showed a poor photovoltaic performance as BO−BO. We believe this can be attributed to a particular interaction at the interface of polymer donor and PCBM acceptor domains in the active layer of photovoltaic devices.[14] For FET devices, only one component, polymer, is present in the active layer. Thus, its performance is mainly determined by the chemical structure and crystalline structure of the polymer. As we mentioned before, DPP units have stronger intermolecular bonding forces than BDT due to the polarity of its lactam groups.[13] Polymer PU−O contains only linear octyl groups on DPP unit, compared with bulky branched alkyl chains for other two polymers. So the linear and small side chain of PU−O facilitates chain packing in the neat film resulting in the best charge carrier mobility among the three polymers. However, for photovoltaic devices, its active layer is a bulk heterojuntion blend of two components, polymer and PCBM. Besides the interaction within each component, the interaction on the interface of the two domains is equally or even more important.[15] As shown in Figure 9, BDT is electron rich and PCBM is electron poor. Intrinsically, there is a tendency for the electron-rich compounds to interact with the electron-poor compounds. The close contact of these two units will benefit the charge separation and transfer at the interface. Calculated from 3D optimized structure, the chain length for each repeat unit of these polymers is ∼20 Å, compared with ∼7 Å for fullerene molecules.[16] This implies that there is enough room for fullerene to contact BDT or DPP unit individually. This intercalation with PCBM was reported to play an important role on the photovoltaic performance.[17] Different side chains on DPP or BDT units in the different polymer will result in a different contact distance between these segments and fullerenes. Polymer O−HD has linear octyl groups on BDT units, so it can create strongest interaction with fullerene than other two polymers with bulky branched chains on BDT units. The closer contact between BDT and fullerene can accelerate electron transfer from polymer to PCBM phase.[18] On the other hand, bimolecular recombination is considered to be a major loss for the V_{oc} and efficiency.[19] The back transfer of electron from fullerene to polymer is more likely to happen between PCBM and electron withdrawing DPP unit in the polymer chain. The bulky 2-hexyldecyl groups on DPP units of O-HD will more efficiently prevent this bimolecular recombination process. However, this effect may not be so evident for the other two polymers due to the smaller side chains on DPP units.

CONCLUSIONS

Three BDT and DPP backboned polymers with different combinations of linear and branched alkyl side chains were synthesized. We systematically investigated the solubility, optical, electrochemical, and solid-state packing properties of these polymers from the view of side chain effect. A more branched side chain will promote solubility but at a cost of decreased crystallinity. FET and PV devices were fabricated with these polymers and we found that a bulky branched side chain on BDT or DPP units shows a dramatically different effect. For FET applications, linear alkyl chains on the electron-deficient DPP units are preferred to offer interchain interaction due to the higher polarity of DPP unit. However, this is not the case for PV applications, where the linear alkyl chains should be moved to electron-rich BDT units with bulky branched alkyl chains to DPP units. It will facilitate the charge separation and transfer at the interface of polymer and PCBM domains, and prevent the electron to flow back to DPP units, which will cause bimolecular charge recombination.

EXPERIMENTAL SECTION

General Methods. UV−vis spectra were measured using a Varian Cary 5000 Spectrometer. Gel permeation chromatography (GPC) (Waters Breeze HPLC system with 1525 Binary HPLC Pump and 2414 Differential Refractometer) was used to measure the molecular weight and polydispersity index at 40 °C with chlorobenzene used as eluent and commercial polystyrenes used as a standard. The differential scanning calorimetry (DSC) analysis of the sample purified by solvent extraction was performed under a nitrogen atmosphere (50 mL/min) using a TA Instrument DSC 2920 at a heating rate of 10 °C/min, calibrated with the melting transition of indium. The thermal gravimetric analysis (TGA) was performed using a TA Instrument TGA 2950 at a heating rate of 10 °C/min under a nitrogen atmosphere (60 mL/min). Cyclic voltammetry (CV) measurements were carried out under argon in a three-electrode cell using 0.1 M Bu_4NPF_6 in anhydrous CH_3CN as the supporting electrolyte with the polymer coated on the platinum-working electrode. The CV curves were recorded with reference to an Ag quasi-reference electrode, which was calibrated using a ferrocene/ferrocenium (Fc/Fc^+) redox couple (4.8 eV below the vacuum level) as an external standard. The $E_{1/2}$ of the Fc/Fc^+ redox couple was found to be 0.42 V vs the Ag quasi-reference electrode. Therefore, the HOMO and LUMO energy levels of the copolymers can be estimated using the empirical equation from $E_{LUMO} = -(E_{os}^{red} + 4.38)$ eV and $E_{HOMO} = -(E_{os}^{ox} + 4.38)$ eV, where E_{os}^{ox} and E_{os}^{red} stand for the onset potentials for the first oxidation and reduction pair relative to the Ag quasi-reference electrode, respectively. X-ray diffraction (XRD) spectrum was

obtained with a Bruker AXS D8 Advance instrument with Co Kα^1 radiation (λ = 1.789 Å). Polymer films casted from the chloroform solution are used for XRD study. Tapping mode AFM image was obtained with a Veeco AFM instrument.

Chemicals. Monomers were synthesized according to the procedure reported in the literature.[11]

General Procedure for Stille Reaction. To a 25 mL flask was added trimethyl tin compound of BDT (0.300 mmol), dibromide monomer of dithienyl DPP (0.300 mmol), and toluene (8 mL). The system was purged with Ar under vacuum. Then $(PPh_3)_4Pd(0)$ (0.06 g, 0.006 mmol) was added in a glovebox. The solution was stirred and refluxed for 24 h under the protection of Ar. After the solution was cooled down to room temperature, the solution was dropped into acetone to precipitate the copolymer. The copolymer was Soxhlet extracted with methanol, acetone, hexanes, dichloromethane, to remove oligmer and then with chloroform to collect the polymer (yield 70−90%). The polymer characterization data are shown in Table 1.

Device Fabrication and Testing. Bottom-contact thin film transistors were fabricated by spin-coating polymer in chloroform (BO−BO and PU−O) or *o*-dichlorobenzene (O−HD) solution on a heavily doped *n*−Si wafer with an overlayer of SiO_2 (230 nm, Ci = 15 nF/cm^2). Gold source and drain electrodes were sputtered on the substrate prior to the deposition of polymer film. The transistor channel length and width are 20 μm and 10 mm, respectively. The current−voltage ($J-V$) characteristics were measured with a computer-controlled semiconductor parameter analyzer (HP4145A) in a N_2 glovebox. The hole mobility was deduced from the saturation regime of the $J-V$ characteristics.

For photovoltaic device fabrication, patterned ITO glass substrates were cleaned with detergent before sonication in CMOS grade acetone and isopropanol for 15 min. The organic residue was further removed by treating with UV-ozone for 10 min. Then a thin layer of PEDOT:PSS (Clevios P, H. C. Starck, 45 nm) was spin-coated and dried for 1 h at 120 °C. A solution of the polymer and PCBM (ADS) in *o*-dichlorobenzene containing different amount of diiodooctane was filtered and spin-coated on top of the PEDOT/PSS layer. The concentration of polymer solution is about 10 mg/mL and weight ratio of polymer to PCBM is 1:2. Spin coating speed is adjusted to 500 to 1500 rpm based on the substrate temperature to get ∼100 nm thick active layer. Then 1.0 nm of LiF and 100 nm Al layer were thermally evaporated through a shadow mask at a pressure of 5×10^{-7} mbar in a Boc Edwards Auto 500 System. The active area is 50 mm^2. The current−voltage ($J-V$) characteristics were measured with a Keithley 2400 digital source meter under simulated air mass (AM) 1.5 solar irradiation of 100 mW cm^{-2} (Sciencetech Inc., SF150). The light intensity was calibrated with a power meter (Gentec Solo PE Laser Power & Energy Meter). The external quantum efficiency (EQE) was performed using a Jobin-Yvon Triax 180 spectrometer, a Jobin-Yvon xenon light source, a Merlin lock-in amplifier, a calibrated Si UV detector, and an SR 570 low noise current amplifier.

AUTHOR INFORMATION

Corresponding Author

*zhao.li@nrc-cnrc.gc.ca (Z.L.),
jianfu.ding@nrc-cnrc.gc.ca (J.D.).

Notes

[§]NRC Publication Number: 52867.

ACKNOWLEDGMENT

We acknowledge financial support from NRC-NSERC-BDC, NRC−CSIC, and NRC-NANO projects.

REFERENCES

(1) (a) Cheng, Y.-J.; Yang, S.-H.; Hsu, C.-S. *Chem. Rev.* **2009**, *109*, 5868. (b) Dennler, G.; Scharber, M. C.; Brabec, C. *J. Adv. Mater.* **2009**, *21*, 1323. (c) Chen, L.-M.; Hong, Z.; Li, G.; Yang, Y. *Adv. Mater.* **2009**, *21*, 1334. (d) Thompson, B. C.; Fréchet, J. M. J. *Angew. Chem., Int. Ed.* **2008**, *47*, 58. (e) Günes, S.; Neugebauer, H.; Sariciftci, N. S. *Chem. Rev.* **2007**, *107*, 1324. (f) Mayer, A. C.; Scully, S. R.; Hardin, B. E.; Rowell, M. W.; McGehee, M. D. *Mater. Today* **2007**, 28. (g) Ong, B. S.; Wu, Y.; Li, Y.; Liu, P.; Pan, H. *Chem.—Eur. J.* **2008**, *14*, 4766. (h) Heeger, A. J. *Chem. Soc. Rev.* **2010**, *39*, 2354. (i) Katz, H. E.; Bao, Z. *J. Phys. Chem. B* **2000**, *104*, 671. (j) Zhao, G.; He, Y.; Xu, Z.; Hou, J.; Zhang, M.; Min, J.; Chen, H.-Y.; Ye, M; Hong, Z.; Yang, Y.; Li, Y. *Adv. Funct. Mater.* **2010**, *20*, 1480.

(2) Chan, H. S. O.; Ng, S. C. *Prog. Polym. Sci.* **1998**, *23*, 1167.

(3) (a) McCullough, R. D.; Lowe, R. D. *J. Chem. Soc., Chem. Commun.* **1992**, 70. (b) Chen, T.-A.; Rieke, R. D. *J. Am. Chem. Soc.* **1992**, *114*, 10087. (c) Loewe, R. S.; Khersonsky, S. M.; McCullough, R. D. *Adv. Mater.* **1999**, *3*, 250.

(4) Gadisa, A.; Oosterbaan, W. D.; Vandewal, K.; Bolsée, J.-C.; Bertho, S.; D'Haen, J.; Lutsen, L.; Vanderzande, D.; Manca, J. V. *Adv. Funct. Mater.* **2009**, *19*, 3300.

(5) Wu, P.-T.; Ren, G.; Jenekhe, S. A. *Macromolecules* **2010**, *43*, 3306.

(6) Hou, J.; Chen, T. L.; Zhang, S.; Huo, L.; Sista, S.; Yang, Y. *Macromolecules* **2009**, *42*, 9217.

(7) (a) Liang, Y.; Xu, Z.; Xia, J.; Tsai, S. -T.; Wu, Y.; Li, G.; Ray, C.; Yu, L. *Adv. Mater.* **2010**, *22*, E135. (b) Wang, E.; Hou, L.; Wang, Z.; Hellström, S.; Zhang, F.; Inganäs, O.; Andersson, M. R. *Adv. Mater.* **2010**, *22*, 5240. (c) Park, S. H.; Roy, A.; Beaupré, S.; Cho, S.; Coates, N.; Moon, J. S.; Moses, D.; Leclerc, M.; Lee, K.; Heeger, A. J. *Nat. Photonics* **2009**, *3*, 297. (d) Hou, J.; Chen, H. -Y.; Zhang, S.; Chen, R. I.; Yang, Y.; Wu, Y.; Li, G. *J. Am. Chem. Soc.* **2009**, *131*, 15586. (e) Piliego, C.; Holcombe, T. W.; Douglas, J. D.; Woo, C. H.; Beaujuge, P. M.; Fréchet, J. M. J. *J. Am. Chem. Soc.* **2010**, *132*, 7595. (f) Zhou, H.; Yang, L.; Price, S. C.; Knight, K. J.; You, W. *Angew. Chem., Int. Ed.* **2010**, *49*, 7992.

(8) (a) Bronstein, H.; Chen, Z.; Ashraf, R. S.; Zhang, W.; Du, J.; Durrant, J. R.; Tuladhar, P. S.; Song, K.; Watkins, S. E.; Geerts, Y.; Wienk, M. M.; Janssen, R. A. J.; Anthopoulos, T.; Sirringhaus, H.; Heeney, M.; McCulloch, I. *J. Am. Chem. Soc.* **2011**, *133*, 3272. (b) Tsao, H. N.; Cho, D. M.; Park, I.; Hansen, M. R.; Mavrinskiy, A.; Yoon, D. Y.; Graf, R.; Pisula, W.; Spiess, H. W.; Müllen, K. *J. Am. Chem. Soc.* **2011**, *133*, 2605. (c) Beaujuge, P. M.; Pisula, W.; Tsao, H. N.; Ellinger, S.; Müllen, K.; Reynolds, J. R. *J. Am. Chem. Soc.* **2009**, *131*, 7514. (d) Li, Y.; Sonar, P.; Singh, S. P.; Soh, M. S.; Meurs, M.; Tan, J. *J. Am. Chem. Soc.* **2011**, *133*, 2198.

(9) (a) Szarko, J. M.; Guo, J.; Liang, Y.; Lee, B.; Rolczynski, B. S.; Strzalka, J.; Xu, T.; Loser, S.; Marks, T. J.; Yu, L.; Chen., L. X. *Adv. Mater.* **2010**, *22*, 5468. (b) Mondal, R.; Ko, S.; Verploegen, E.; Becerril, H. A.; Toney, M. F.; Bao, Z. *J. Mater. Chem.* **2011**, *21*, 1537. (c) Yang, L; Zhou, H.; You, W. *J. Phys. Chem. C* **2010**, *114*, 16793. (d) Wang, E.; Hou, L.; Wang, Z.; Ma, Z.; Hellström, S.; Zhuang, W.; Zhang, F.; Inganäs, O.; Andersson, M. R. *Macromolecules* **2011**, *44*, 2067. (e) Egbe, D. A. M.; Nguyen, L. H.; Hoppe, H.; Mühlbacher, D.; Sariciftci, S. S. *Macromol. Rapid Commun.* **2005**, *26*, 1389. (f) Yang, M.; Peng, B.; Liu, B.; Zou, Y.; Zhou, K.; He, Y.; Pan, C.; Li, Y. *J. Phys. Chem. C* **2010**, *114*, 17989. (g) Biniek, L.; Fall, S.; Chochos, C. L.; Anokhin, D. V.; Ivanov, D. A.; Leclerc, N.; Lévêque, P.; Heiser, T. *Macromolecule* **2010**, *43*, 9779.

(10) (a) Wienk, M. M.; Turbiez, M.; Gilot, J.; Janssen, R. A. J. *Adv. Mater.* **2008**, *20*, 2556. (b) Walker, B.; Tamayo, A. B.; Dang, X.-D.; Zalar, P.; Seo, J. H.; Garcia, A.; Tantiwiwat, M.; Nguyen, T.-Q. *Adv. Funct. Mater.* **2009**, *19*, 3063. (c) Zou, Y.; Gendron, D.; Badrou-Aïch, R.; Najari, A.; Tao, Y.; Leclerc, M. *Macromolecules* **2009**, *42*, 6361.

(11) (a) Zhou, E.; Yamakawa, S.; Tajima, K.; Yang, C.; Hashimoto, K. *Chem. Mater.* **2009**, *21*, 4055. (b) Tamayo, A. B.; Tantiwiwat, M.; Walker, B.; Nguyen, T.-Q. *J. Phys. Chem. C* **2008**, *112*, 15543. (c) Li, Z.; Lu, J.; Tse, S.-C.; Zhou, J.; Du, X.; Tao, Y.; Ding, J. *J. Mater. Chem.* **2011**, *21*, 3226. (d) Hou, L.; Hou, J.; Chen, H.-Y.; Zhang, S.; Jiang, Y.; Chen, T. L.; Yang, Y. *Macromolecules* **2009**, *42*, 6564.

(12) (a) Bavel, S. V.; Veenstra, S.; Loos, J. *Macromol. Rapid Commun.* **2010**, *31*, 1835. (b) Yang, X.; Loos, J. *Macromolecules* **2007**, *40*, 1353. (c) Giridharagopal, R.; Ginger, D. S. *J. Phys. Chem. Lett.* **2010**, *1*, 1160.

(13) Hao, Z.; Iqbal, A. *Chem. Soc. Rev.* **1997**, *26*, 203.

(14) Venkataraman, D.; Yurt, S.; Venkatraman, B. H.; Gavvalapalli, N. *J. Phys. Chem. Lett.* **2010**, *1*, 947.

(15) (a) Steim, R.; Kogler, F. R.; Brabec, C. J. *J. Mater. Chem.* **2010**, *20*, 2499. (b) Chen, L.-M.; Xu, Z.; Hong, Z.; Yang, Y. *J. Mater. Chem.* **2010**, *20*, 2575.

(16) Goel, A.; Howard, J. B.; Sande, J. B. V. *Carbon* **2004**, *42*, 1907.

(17) Cates, N. C.; Gysel., R.; Beiley, Z.; Miller, C. E.; Toney, M. F.; Heeney, M.; McCulloch, I.; McGehee, M. D. *Nano Lett.* **2009**, *9*, 4153.

(18) Clarke, T. M.; Durrant, J. R. *Chem. Rev.* **2010**, *110*, 6736.

(19) (a) Vandewal, K.; Tvingstedt, K.; Gadisa, A.; Inganäs, O.; Manca, J. V. *Nat. Mater.* **2009**, *8*, 904. (b) Koster, L. J. A.; Wienk, M. M.; Maturová, K.; Janssen, R. A. *J. Adv. Mater.* **2011**, *23*, 1670. (c) Maurano, A.; Hamilton, R.; Shuttle, C. G.; Mallantyne, A. M.; Nelson, J.; O'Regan, B.; Zhang, W.; McCulloh, I.; Azimi, H.; Morana, M.; Brabec, C. J.; Durrant, J. R. *Adv. Mater.* **2010**, *22*, 4987.